Development 138, 4207-4217 (2011) doi:10.1242/dev.064444

HP1γ links histone methylation marks to meiotic synapsis in mice

Yuki Takada[1,*], Chie Naruse[2,*], Yael Costa[3,*], Takayuki Shirakawa[4], Makoto Tachibana[5], Jafar Sharif[1], Fuyuko Kezuka-Shiotani[1], Dai Kakiuchi[2], Hiroshi Masumoto[6], Yo-ichi Shinkai[5], Kazuyuki Ohbo[4], Antoine H. F. M. Peters[7], James M. A. Turner[3], Masahide Asano[2,†] and Haruhiko Koseki[1,8,†]

SUMMARY

During meiosis, specific histone modifications at pericentric heterochromatin (PCH), especially histone H3 tri- and dimethylation at lysine 9 (H3K9me3 and H3K9me2, respectively), are required for proper chromosome interactions. However, the molecular mechanism by which H3K9 methylation mediates the synapsis is not yet understood. We have generated a *Cbx3*-deficient mouse line and performed comparative analysis on *Suv39h1/h2*-, *G9a*- and *Cbx3*-deficient spermatocytes. This study revealed that H3K9me2 at PCH depended on Suv39h1/h2-mediated H3K9me3 and its recognition by the *Cbx3* gene product HP1γ. We further found that centromere clustering and synapsis were commonly affected in *G9a*- and *Cbx3*-deficient spermatocytes. These genetic observations suggest that HP1γ/G9a-dependent PCH-mediated centromere clustering is an axis for proper chromosome interactions during meiotic prophase. We propose that the role of the HP1γ/G9a axis is to retain centromeric regions of unpaired homologous chromosomes in close alignment and facilitate progression of their pairing in early meiotic prophase. This study also reveals considerable plasticity in the interplay between different histone modifications and suggests that such stepwise and dynamic epigenetic modifications may play a pivotal role in meiosis.

KEY WORDS: HP1γ, PCH, Synapsis, Centromere clustering, Mouse

INTRODUCTION

Eukaryotes produce viable gametes for sexual reproduction by meiosis, during which the genetic material can be interchanged between paternal and maternal chromosomes and the DNA content of the precursor cell is halved by two successive cell divisions. The meiotic process in most organisms comprises pairing, synapsis, recombination and two successive meiotic divisions. In virtually all organisms, the homologous chromosomes pair along their length, connected along the entire length by the synaptonemal complex and eventually become locked together by recombination. Previous genetic studies mainly in plants, *Drosophila*, fission and budding yeast shed light on the role of centromeric heterochromatin in homolog pairing and synapsis (Prieto et al., 2004; Dernburg et al., 1996; Ding et al., 2004; Kemp et al., 2004; Tsubouchi and Roeder, 2005). Intriguingly, recent studies in budding yeast suggest that centromere pairing occurs in a sequence-independent manner and involves a non-homologous association and re-sorting processes that couples homologous centromeres (Tsubouchi and Roeder, 2005). Therefore sequence-independent recognition of centromeric regions appears to be a crucial early step in creating meiotic chromosome associations. This model leads to the prediction that this centromere pairing involves chromatin proteins that probably give rise to pericentric heterochromatin (PCH).

Based on previous genetic studies, epigenetic regulation at PCH is suggested to play a crucial role in meiotic prophase. SET-domain proteins, Suv39h1 and Suv39h2, which mediate H3K9me3 at PCH, were shown to be involved in chromosome interactions and subsequent segregation during meiosis (Peters et al., 2001). Another histone methyl transferase (HMTase), G9a, which mediates transient H3K9me2 deposition at PCH during early meiotic prophase, was also shown to be required for synchronous synapsis (Tachibana et al., 2007) (see Fig. S1 in the supplementary material). However, the molecular mechanism by which H3K9 methylation mediates the synapsis is not yet understood.

This study is thus designed to clarify how the functions of two different H3K9 methylation marks are linked and integrated to mediate synapsis during the meiotic prophase. To this end, we focused on heterochromatin protein 1 (HP1) family proteins – evolutionarily conserved chromo-domain proteins that are involved in recognition of H3K9 methylation and localize to heterochromatic regions, including PCH (Metzler-Guillemain et al., 2003; Cheutin et al., 2003; Pidoux and Allshire, 2005). HP1 proteins are also essential for heterochromatin silencing in various organisms and do so by recruiting a vast range of effector molecules (Nakayama et al., 2001; Jenuwein and Allis, 2001; Bannister et al., 2001). HP1 proteins in mammals have three isotypes, HP1α (encoded by *Cbx5*), HP1β (encoded by *Cbx1*) and HP1γ (encoded by *Cbx3*) (Lomberk et al., 2006). It is noteworthy that HP1γ has been shown to form complexes with G9a (Ogawa et al., 2002). Based on genetic studies in *Drosophila*, mutations in the HP1 protein, which localizes to PCH, eliminate repression of marker genes lying in close proximity to centromeric heterochromatin and cause defective chromosome segregation (Kellum and Alberts, 1995). It has also been reported

[1]RIKEN Center for Allergy and Immunology, 1-7-22 Suehiro-cho, Tsurumi-ku, Yokohama 230-0045, Japan. [2]Advanced Science Research Center, Kanazawa University, 13-1 Takara-machi, Kanazawa 920-8640, Japan. [3]Division of Stem Cell Biology and Developmental Genetics, MRC NIMR, The Ridgeway, Mill Hill, London NW7 1AA, UK. [4]Department of Histology and Cell Biology, School of Medicine, Yokohama City University, 3-9 Fukuura, Kanazawa-ku, Yokohama 236-0004, Japan. [5]Graduate School of Biostudies, Kyoto University, 53 Shogoin, Kawara-cho, Sakyo-ku, Kyoto 606-8507, Japan. [6]Laboratory of Cell Engineering, Department of Human Genome Research, Kazusa DNA Research Institute, Kisarazu, Chiba 292-0818, Japan. [7]Friedrich Miesher Institute for Biomedical Research, Maulbeerstrasse 66, CH-4058 Basel, Switzerland. [8]Core Research for Evolutional Science and Technology (CREST), Japan Science and Technology Corporation (JST), Tokyo 240-0193, Japan.

*These authors contributed equally to this work
[†]Author for correspondence (asano@kiea.m.kanazawa-u.ac.jp; koseki@rcai.riken.jp)

Accepted 18 July 2011

that in the fission yeast, mutations of silencing factors *clr4*$^{+}$ and *rik1*$^{+}$ disrupt the localization of the Swi6p (a yeast homolog of HP1) and cause impairment of centromeric functions (Ekwall et al., 1996). Together, these observations suggest that the HP1 family of proteins may have a functional role, for example, to link Suv39h1/h2 and G9a via H3K9me3 recognition at the PCH for the progression of meiotic prophase.

To test this hypothesis, we isolated a mutant *Cbx3* allele and performed a comparative genetic approach using mice deficient for *Suv39h1/h2*, *G9a* and *Cbx3*. Our study revealed that H3K9me2 at PCH depended on Suv39h1/h2-mediated H3K9me3 and on its recognition by HP1γ. We further found that centromere clustering and synapsis were commonly affected in *G9a*- and *Cbx3*-deficient spermatocytes. These genetic observations suggest that HP1γ/G9a-dependent PCH-mediated centromere clustering is an axis for correct chromosome interactions during meiotic prophase.

MATERIALS AND METHODS

Mice

Cbx3-KO mice were generated by the gene trap method described previously (Naruse et al., 2007). To determine the genotype of mutant mice, genomic PCR was performed using *Cbx3*_F (5′-GAGTGATT-ACCGACACCACCA-3′) and *Cbx3*_R (5′-TTTAATCGGAGACTTG-AAGAGC-3′) in intron 1 for the wild-type allele, and *Cbx3*_F and primer 3 (5′-GTTCGCTTCTCGCTTCTGTT-3′) in the trap vector for the mutant allele. Briefly, *Suv39h1/2* double null mice were maintained on a mixed genetic background of 129/Sv and C57Bl/6J origin (Peters et al., 2001). Double heterozygotes were mated to generate double homozygotes. *G9a* conditional allele was also maintained on a mixed genetic background of 129/Sv and C57Bl/6J origin (Tachibana et al., 2007). Briefly, germline-specific *G9a*-KO mice were generated by crossing *G9a*$^{flox/flox}$ females with *TNAP-Cre, G9a*$^{+/flox}$ males.

Immunofluorescence of meiotic cell spreads and testes sections

For immunofluorescence analysis, germ cells were isolated from male and female mice of each genotype and prepared using a ‘drying-down’ technique (Peters et al., 1997) with the following modifications. To obtain the germ cells, testes were shredded by needles in phosphate-buffered saline (PBS) supplemented with 10% fetal bovine serum (FBS). Cell suspension was filtered with 100 μm and 50 μm mesh to remove the debris. After centrifugation, cells were placed in 100 μl of hypotonic extraction buffer for 8 minutes. After several washes with PBS, we adjusted the germ cell number to 1×10^{7}/ml. Cell suspension (10 μl) was mixed with 10 μl of sucrose solution and then placed on glass slides that had been dipped in fixation solution. After the cell suspension was slowly dispersed, the slides were dried for 1 hour in a closed box with high humidity and then for 30 minutes in an opened box. After preparation, slides bearing cell spreads were processed using standard procedures. The antibodies used for immunofluorescence analysis in this study were: anti-dimethyl-Histone H3(Lys9), rabbit, 1:100, Millipore; anti-dimethyl-Histone H3(Lys9), mouse, 1:300, Abcam; anti-trimethyl-Histone H3(Lys9), rabbit, 1:100, Millipore; anti-trimethyl-Histone H3(Lys9), mouse, 1:300, Abcam; anti-SYCP3, rabbit, 1:300, NOVUS; anti-SYCP3, mouse, 1:300, NOVUS; anti-SYCP1, rabbit, 1:250, NOVUS; anti-HP1γ, mouse, 1:50, USBiological; anti-HP1β, rat, 1:50, Serotec; anti-HP1α, mouse, 1:50, Euromedex; anti-G9a, mouse, 1:50, PPMX; anti-centromere antibody (ACA), human, 1:50 (Muro et al., 1991); CREST, mouse, 1:500, a gift from Dr Earnshaw (Edinburgh University, UK); Mvh, mouse, 1:100, Upstate; anti-phospho-H2A.X(Ser139), rabbit, 1:300, Millipore; anti-ATR, goat, 1:50, Santa Cruz; anti-trimethyl-Histone H4(Lys20), rabbit, 1:100, Biolegend; anti-Kit, rat, 1:10, eBioscience; anti-Plzf, rabbit, 1:300, Santa Cruz; anti-mouse IgG(H+L) Alexa 488, goat, 1:300, Invitrogen; anti-mouse IgG(H+L) Alexa 568, goat, 1:300, Invitrogen; anti-mouse IgG(H+L) Alexa 647, goat, 1:300, Invitrogen; anti-rabbit IgG(H+L) Alexa 488, goat, 1:300, Invitrogen; anti-rabbit IgG(H+L) Alexa 568, goat, 1:300, Invitrogen; anti-rabbit IgG(H+L) Alexa 647, goat, 1:300, Invitrogen; anti-rat IgG(H+L) Alexa 568, goat, 1:300, Invitrogen; anti-human IgG(H+L) Alexa 488, goat, 1:300, Invitrogen; anti-rat IgG(H+L) Alexa 488, donkey, 1:300, Invitrogen. Testes were fixed overnight in Bouin’s solution, embedded in paraffin and sectioned. After preparation, specimens were processed for immunofluorescence using standard procedures.

TUNEL staining

Testes sections were prepared as described above. Apoptotic cells were visualized by the terminal deoxynucleotidetransferase-mediated dUTP nick end-labeling (TUNEL) assay (In Situ Cell Death Detection Kit, AP; Roche, Germany).

Immunofluorescent in situ hybridization analysis

DNA fluorescent in situ hybridization was carried out after immunofluorescence with anti-SYCP1, anti-SYCP3 and anti-H3K9me3 antibodies. We used digoxigenin, Alexa488 and/or Cy3-labeled probes, prepared using a Nick Translation Kit (Roche), and hybridizations were carried out as previously described (Nakashima et al., 2005) with the following slight modifications. First, for a digoxigenin-labeled minor satellite specific probe, slides were re-fixed in 2% paraformaldehyde (PFA) for 10 minutes, then rinsed in PBS, dehydrated through an ethanol series (70%, 80%, 90% and 100%) and air dried. After the slides were dipped in 2× SSC buffer, they were denatured at 73°C for 3 minutes and dehydrated through a cold ethanol series (twice for 70%, 80%, 90% and 100%) and air dried. Hybridization reactions were carried out in humid chambers for 2 hours at 37°C. The slides were subjected to stringency washes at 37°C (twice with 2× SSC and 50% formamide, twice with 2× SSC) and then blocked (4× SSC and 5% skim milk) for 1 hour before probe detection. Probe detection was carried out using rhodamine-labeled anti-DIG antibody. Incubations were for 1 hour and slides were washed in 4× SSC and 0.1% TritonX-100. For the Cy3-labeled Chr2-Cen (BAC RP23-60E18) and Alexa488-labeled Chr4-Mid (Cosmid WI1-870P20) probes, slides were re-fixed in 4% PFA for 10 minutes, then rinsed in PBS and incubated in PBS supplemented with 20% glycerol. After four cycles of freeze-thawing in liquid nitrogen, we incubated the slides in 0.1 N HCl for 10 minutes. After the slides were dipped in 2× SSC buffer at room temperature and 2× SSC and 50% formamide at 4°C, they were denatured at 73°C for 5 minutes, dehydrated through a cold ethanol series (twice for 70%, 80%, 90% and 100%) and air dried. Hybridization reactions were carried out in humid chambers overnight at 37°C. We then subjected the slides to stringency washes at 42°C (twice with 2× SSC and 50% formamide, twice with 2× SSC and 0.1% Tween20) and PBS at room temperature.

Quantitative RT-PCR and bisulfite DNA sequencing analyses

Total RNA for quantitative RT-PCR analysis and genomic DNA for bisulfite DNA sequencing analysis were isolated from the testicular germ cells of 2-week-old *Cbx3* heterozygous and homozygous mutant mice. We performed these analyses as described previously (Sharif et al., 2007).

Whole-mount immunofluorescence

The whole-mount immunohistochemical analysis was performed as reported previously (Ohmura et al., 2004). The antibodies used for whole-mount immunostaining are listed above.

RESULTS

H3K9me2 at PCH depends on Suv39h1/2 during meiotic prophase

To examine the link between Suv39h1/2 and G9a during meiotic prophase, we compared subnuclear localization of H3K9me3 and H3K9me2 and spermatogenetic defects in respective mutants. We found that H3K9me2 colocalized with H3K9me3 at the PCH intensely at the leptotene, but only weakly at the pachytene and diplotene stages (see Fig. S2 in the supplementary material) (Peters et al., 2001; Tachibana et al., 2007). Although H3K9me2 signals in the pachytene spermatocytes were much weaker than leptotene and zygotene, these were specific as we did not observe any signals in *G9a*-KO spermatocytes (Y.T., unpublished) (Khalil et al., 2004).

By using immunofluorescent in situ hybridization analysis for SYCP3 and SYCP1 proteins (Lammers et al., 1994; Meuwissen et al., 1992) and centromeric repeats, we observed that the meiotic defects in *G9a*-KO mice resembled those observed previously in *Suv39h* dominant-negative (dn) mice and most probably represent defects in the pairing of homologous chromosomes at early meiotic prophase (Peters et al., 2001) (Table 1; see Fig. S1 in the supplementary material). These results suggest that G9a may functionally be linked to Suv39h1/h2 to mediate the synapsis.

We went on to determine how the activities of G9a and Suv39h1/h2 are linked. Previous studies showed that inactivation of G9a did not perturb H3K9me3 in meiotic cells in male mice (Tachibana et al., 2007). We, therefore, asked whether disruption of H3K9me3 impairs H3K9me2 deposition. We analyzed the H3K9me2 pattern in meiotic spermatocytes from *Suv39h* (dn) mice and found the expected H3K9me3 defect in *Suv39h* dn spermatocytes as previously reported (Peters et al., 2001). This was accompanied by severe impairment of H3K9me2 deposition, particularly at the PCH, in leptotene spermatocytes (Fig. 1A). Quantitative analysis for immunofluorescence intensity revealed ~40% loss in H3K9me2 labeling in *Suv39h* dn spermatocytes (*n*=60) (Fig. 1B). These data suggest that pericentric deposition of H3K9me2 at early meiotic prophase requires pre-existing H3K9me3, but not vice versa, and therefore establish an epigenetic cascade progressing from Suv39h to G9a HMTases to mediate the synapsis.

HP1γ localization at PCH depends on H3K9me3 catalyzed by Suv39h1/h2

We went on to address the molecular mechanisms that link Suv39h to G9a. The HP1 family includes the key proteins that recognize methylated H3K9 at heterochromatic regions via their evolutionarily conserved chromodomain and, therefore, are attractive candidates for this role. Indeed, in mammalian cells H3K9me3 catalyzed by the Suv39h1/h2 enzymes has been shown to create a binding platform for HP1 at PCH (Lachner et al., 2001). Another study reported delocalization of HP1γ from PCH in *Suv39h* dn B-spermatogonia (Peters et al., 2001). These findings support our hypothesis that HP1 is linked to epigenetic modifications of H3K9 at PCH.

HP1 proteins in mammals have three isotypes, HP1α, HP1β and HP1γ. In order to identify the most likely candidate(s), we performed immunofluorescent analysis to detect colocalization of HP1α, HP1β and HP1γ with SYCP3 during meiotic prophase, consistent with previous findings in human testis (Metzler-Guillemain et al., 2003). HP1γ was present within broad domains of the PCH, in which different numbers of centromeres were clustered, from leptotene until just before the first meiotic division (see Fig. S3A in the supplementary material). By contrast, HP1β at the PCH was only weakly detected at leptotene, becoming more clearly visible beginning with the zygotene stage (see Fig. S3B in the supplementary material). Bright focal distributions of HP1α were not detected at the leptotene stage but appeared at pachytene (see Fig. S3C in the supplementary material). These findings suggest that among HP1 family members, HP1γ is involved in the recognition of pericentric H3K9me3 at early meiotic prophase.

To further analyze the role of HP1γ in linking Suv39h1/h2 and G9a, we next performed a comparative analysis of the pericentric deposition of HP1γ in *Suv39h* dn and *G9a*-KO spermatocytes at early meiotic prophase. Quantitative immunofluorescence analysis revealed approximately 60% reduction of pericentric HP1γ deposition in *Suv39h* dn spermatocytes (*n*=60) (Fig. 1C). By contrast, obvious reduction of HP1γ deposition was not seen in *G9a*-KO spermatocytes (*n*=50) (Fig. 1D). These findings suggest that HP1γ participates in the recognition of H3K9me3 at PCH and, therefore, suggest that HP1γ is a strong candidate as a molecular linker for H3K9me3 and H3K9me2 to mediate proper meiotic synapsis.

Table 1. Morphological alterations seen in pachytene spermatocytes in *Cbx3*- and *G9a*-KO mice at 15 dpp

	Frequency of chromosomes with respective phenotypes (%)		
Phenotypes	Wild type	*Cbx3*-KO	*G9a*-KO
Asynapsis of entire chromosomes	0.1	5.8	5.9
Asynapsis at the telocentric regions	0.3	16.5	10
Asynapsis at the middle regions	0.3	0.7	0.4
Asynapsis at the telomeric regions	0.3	2.8	3.1
Normal	99	74.2	80.6

Based on five categories of synaptic defects, we scored the frequency of chromosomes at pachytene stage spermatocytes in wild type (wt), *Cbx3*-KO and *G9a*-KO. The numbers of spermatocytes analyzed were as follows: wild type, *n*=154 from seven mice; *Cbx3*-KO, *n*=97 from three mice; *G9a*-KO, *n*=99 from two mice at 15 dpp.

Meiotic catastrophe in *Cbx3*-deficient spermatocytes

We went on to analyze the role of HP1γ during meiosis by taking advantage of a gene-trap mutation where there has been a single insertion of a trap vector into the first intron of the *Cbx3* gene (see Fig. S4 in the supplementary material). This insertion impairs the expression of *Cbx3* in homozygous mutant mice (*Cbx3*-KO). As the *Cbx3* genomic locus includes the divergently transcribed *Hnrnpa2b1* gene, it is possible that transcription of this gene is concurrently affected by this insertion (Sato et al., 2001; Williams et al., 2005). We thus checked the expression of *Hnrnpa2b1* and found it was unaffected in *Cbx3*-KO (C.N. and M.A., unpublished). We used mixed genetic background (C57BL/6 and 129/Ola) to generate viable homozygous *Cbx3*-KO mice as *Cbx3*-KO mice on a C57BL/6 background exhibited neonatal lethality (Y.T., unpublished observations). With this compound background, homozygous mutants appeared in a similar ratio as previously reported and displayed growth retardation (Brown et al., 2010) (Y.T., unpublished).

We found that all *Cbx3*-KO males and most females were infertile with a single exception among more than 50 *Cbx3*-KO females, which gave birth to a single offspring after natural mating. Brown and colleagues also reported a similar result that the one adult $Cbx3^{hypo/hypo}$ female analyzed in their study had normal ovaries, although that female was sterile (Brown et al., 2010). Consistent with these reproductive defects, testes and ovaries from *Cbx3*-KO mice were reduced in size (Fig. 2A; Y.T., unpublished). In male mutants, we observed severe depletion of spermatocytes and post-meiotic cells (Fig. 2B). Accumulation of zygotene and pachytene spermatocytes was particularly affected in the *Cbx3*-KO mice (Fig. 2C). Careful histological analysis further revealed reduction of late leptotene spermatocytes (C.N., unpublished). These defects were associated with extensive apoptotic outbursts of germ cells in the seminiferous tubules (Fig. 2D). Taken together, we suggest that considerable numbers of *Cbx3*-KO spermatocytes are progressively deleted during early meiotic prophase.

To better understand the impaired meiotic phenotypes of the *Cbx3*-KO male mice, we checked meiotic synapsis by immunofluorescent in situ hybridization analysis (Fig. 2E). All

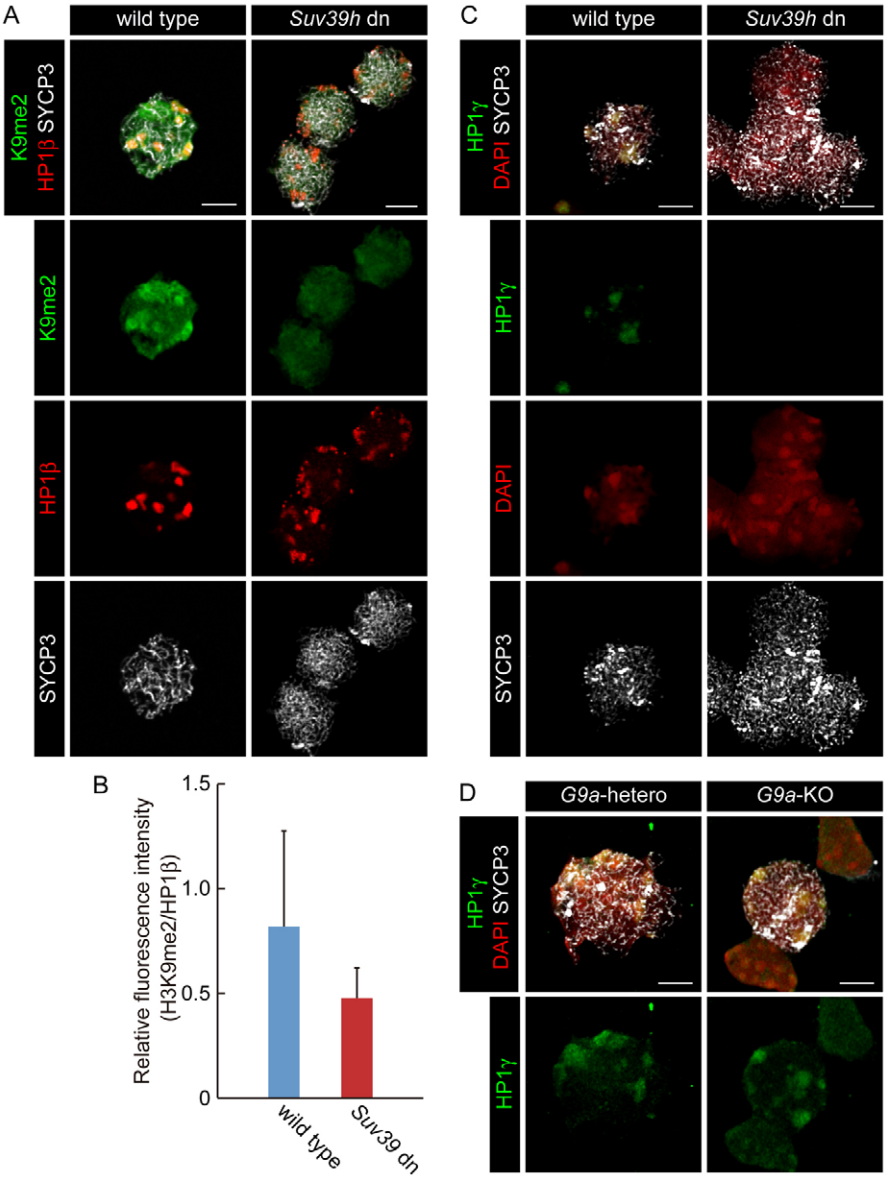

Fig. 1. G9a is functionally linked to Suv39h1/h2 during meiotic prophase. (**A**) Significant reduction of H3K9me2 distribution at the PCH in *Suv39h* dn spermatocytes. Immunofluorescence analysis for H3K9me2 (K9me2; green), HP1β (red) and SYCP3 (white) in wild-type and *Suv39h* dn spermatocytes at the leptotene stage. The numbers of spermatocytes analyzed were as follows: wild type, *n*=60 from two mice; *Suv39h* dn, *n*=60 from two mice at 15 dpp. Scale bars: 5 μm. (**B**) Quantitative analysis of immunofluorescence intensity of H3K9me2 between wild-type and *Suv39* dn spermatocytes. Relative fluorescence intensity of H3K9me2 against HP1β at PCH in *Suv39* dn was significantly reduced compared with wild type. The numbers of spermatocytes analyzed were as follows: wild type, *n*=89 from two mice; *Suv39h* dn, *n*=60 from two mice at 15 dpp. The significance of the difference was evaluated using Student's *t*-test (P=9.62E^{-08}). Data are mean±s.e.m. (**C**) Suv39h1/h2-dependent distribution of HP1γ at the PCH. Immunofluorescence analysis for HP1γ (green) and SYCP3 (white) with DAPI counterstaining (red) in wild-type and *Suv39h* dn spermatocytes at the leptotene stage. The numbers of spermatocytes analyzed were as follows: wild type, *n*=72 from two mice; *Suv39h* dn, *n*=60 from two mice at 15 dpp. Scale bars: 5 μm. (**D**) G9a-independent distribution of HP1γ at PCH. Immunofluorescence analysis for HP1γ (green) and SYCP3 (white) with DAPI counterstaining (red) in *G9a*-hetero and *G9a*-KO spermatocytes at the leptotene stage. The numbers of spermatocytes analyzed were as follows: *G9a*-hetero, *n*=50 from two mice; *G9a*-KO, *n*=50 from two mice at 15 dpp. Scale bars: 5 μm.

Cbx3-KO cells (100%; *n*=97) showed some degree of asynapsis, affecting the autosomes or sex chromosomes, or both (Table 1). Synaptic failures in *Cbx3*-KO mice were further confirmed by dual staining with antibodies to SYCP3 and phosphorylated H2A.X (γH2AX) or ATR. *Cbx3*-KO spermatocytes with extensive asynapsis showed diffuse γH2AX and discontinuous ATR staining of unsynapsed chromosomes (see Fig. S5 in the supplementary material). A similar effect of *Cbx3* loss on germ cell development and chromosome synapsis was seen in females (see Fig. S6A in the supplementary material). *Cbx3*-KO females exhibited severe and progressive depletion of oocytes during meiotic prophase and synaptic failures as revealed by immunostaining for γH2AX (see Fig. S6B,C in the supplementary material). Asynapsis to various extents was observed in 25% of chromosomes in *Cbx3*-KO pachytene spermatocytes whereas 75% of chromosomes normally synapsed (Table 1). These observations imply that HP1γ is dispensable for the synapsis but facilitates this process.

Interestingly, the asynaptic phenotype in *Cbx3*-KO pachytene spermatocytes occurred preferentially at the centromeric ends of the chromosome pairs (Fig. 2E; Table 1). Close examination of bivalents in the mutants that had undergone apparently normal synapsis revealed a centromeric abnormality, with a proportion of the homologous centromeric signals being staggered rather than showing complete colocalization, indicating a defect in the condensation of PCH (Fig. 2E,F). Consistent with these structural alterations involving centromeres, we observed various chromosomal aberrations that potentially emanated from defects in the pairing of homologous chromosomes, such as heterophilic interactions of chromosomal ends and univalency of homologous and sex chromosomes (Y.T. and Y.C., unpublished). These findings suggested that *Cbx3*-deficiency impaired the functions of PCH in the early meiotic prophase. These defects in *Cbx3*-KO meiotic germ cells were similar to those seen in *Suv39h* dn and *G9a*-KO mice (Peters et al., 2001; Tachibana et al., 2007), suggesting that the role of HP1γ is to link H3K9me3 with H3K9me2 at PCH.

Recruitment of G9a to PCH depends on HP1γ

We went on to test whether HP1γ is involved in the H3K9me2 modification at PCH by using immunofluorescence analysis. We indeed observed significant reduction of H3K9me2 levels at the

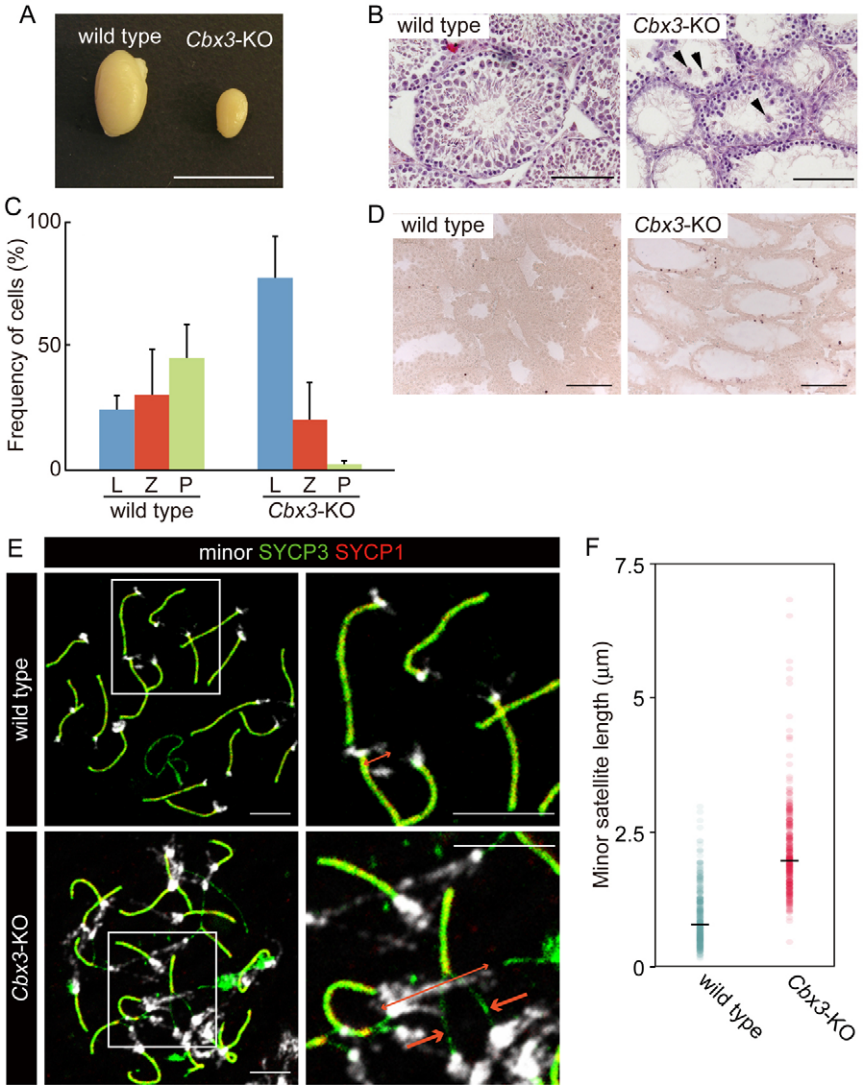

Fig. 2. Defects in spermatogenesis in *Cbx3* mutants occur at early meiotic prophase. (**A**) Testis hypoplasia seen in 8-week-old *Cbx3*-KO mouse. Scale bar: 1 cm. (**B**) Reduction of spermatocytes in *Cbx3*-KO mice. Cross-sections of testes from 4-week-old wild type and *Cbx3*-KO are shown. Sections were stained with Hematoxylin and Eosin. The *Cbx3*-KO section reveals many seminiferous tubules that lack germ cells, accompanied by the appearance of morphologically abnormal spermatocytes indicated by arrowheads. Scale bars: 100 μm. (**C**) Spermatogenic defects in the *Cbx3*-KO at early meiotic prophase. Developmental profiles of meiotic spermatocytes in wild type and *Cbx3*-KO at 16 dpp are graphically depicted. Frequency of leptotene (L), zygotene (Z) and pachytene (P) spermatocytes are shown by blue, red and green bars, respectively. The significance of the difference between wild-type and *Cbx3*-KO at leptotene and pachytene spermatocyte was evaluated using Student's *t*-test (leptotene; P=0.005, pachytene; P=0.008). The numbers of spermatocytes analyzed were as follows: wild type, n=382 from four mice; *Cbx3*-KO, n=234 from three mice. Data are mean±s.e.m. (**D**) Increased apoptotic spermatocytes in *Cbx3*-KO testes. Incidence of apoptosis was examined in wild-type and *Cbx3*-KO testes at day 19 dpp by TUNEL labeling. In *Cbx3*-KO testes, a significant number of TUNEL-labeled cells were observed in the thinned layers of seminiferous tubules. Scale bars: 100 μm. (**E**) Meiotic catastrophe in *Cbx3*-KO spermatocytes. Immunofluorescent in situ hybridization results for SYCP3 (green) and SYCP1 (red) proteins and satellite repeats (minor; white) in wild type and *Cbx3*-KO are shown. Higher magnification views (indicated by boxes in the left panels) are shown in the right panels for each genotype. Red double-headed arrows show the ranges of minor satellite signals; red arrows show the asynapsis at the telocentric region. Scale bars: 5 μm. (**F**) Quantitative analysis of minor satellite repeats length between wild-type and *Cbx3*-KO spermatocytes. Minor satellite repeats were significantly elongated in *Cbx3*-KO compared with wild type. The numbers of spermatocytes analyzed were as follows: wild type, n=360 from two mice; *Cbx3*-KO, n=330 from two mice at 15 dpp. Each dot represents an observed length of minor satellite and horizontal line represents median of the distribution. The significance of the difference was evaluated using Student's *t*-test (P=5.15E^{-80}).

PCH in *Cbx3*-KO cells during meiotic prophase, suggesting that acquisition of this mark at the PCH depends on HP1γ (Fig. 3A,B; see Fig. S7 in the supplementary material). By contrast, obvious differences in H3K9me2 levels were not seen outside the PCH between the wild type and *Cbx3*-KO. Consistent with this, we found several G9a target genes still repressed in *Cbx3*-KO spermatocytes (Y.T., unpublished). These observations suggest that HP1γ mediates H3K9me2 at PCH by recognizing H3K9me3. Consistently, loss of HP1γ did not affect pericentric deposition of H3K9me3 in *Cbx3*-KO spermatocytes (Fig. 3C).

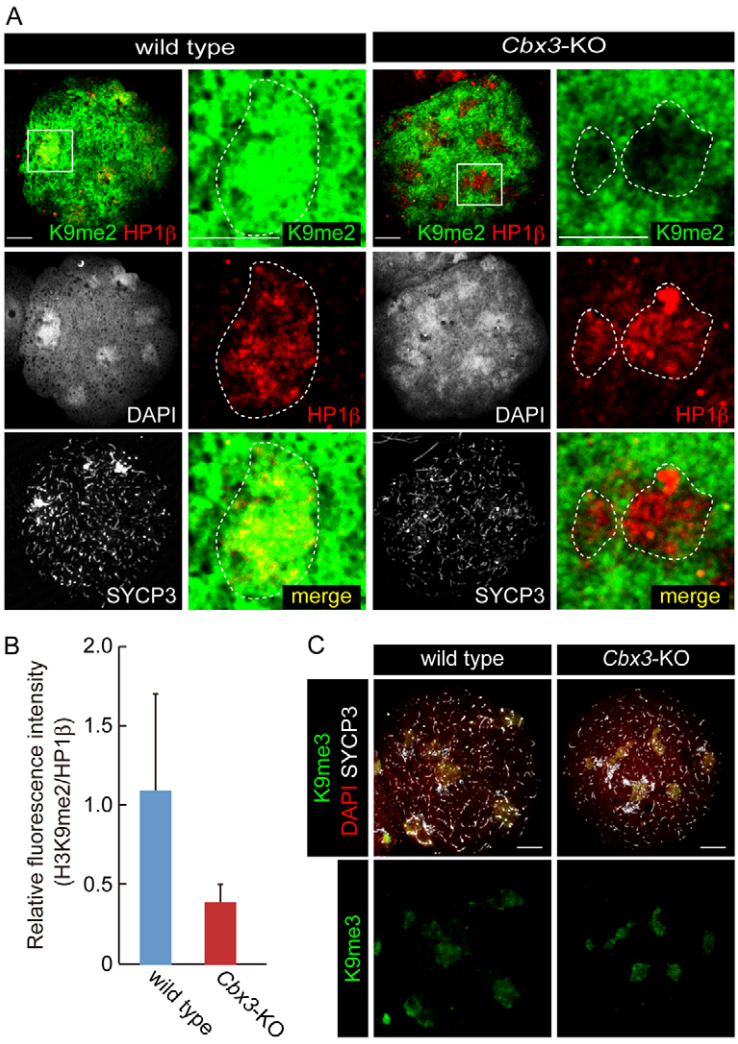

Fig. 3. Requirement for HP1γ to mediate H3K9me2 by recruiting G9a to pericentric heterochromatin during meiotic prophase. (**A**) Failure of H3K9me2 deposition at PCH at the leptotene stage in *Cbx3*-KO spermatocytes. Immunofluorescence results for H3K9me2 (K9me2; green), HP1β (red) and SYCP3 (white) with DAPI counterstaining (white) in wild type and *Cbx3*-KO at the leptotene stage. Higher magnification views for the PCH (indicated by boxes in the upper panels) are shown in lower panels for each genotype. The PCH is indicated by broken lines. The numbers of spermatocytes analyzed were as follows: wild type, *n*=145 from three mice; *Cbx3*-KO, *n*=150 from three mice at 15 dpp. Scale bars: 5 μm. (**B**) Quantitative analysis of immunofluorescence intensity of H3K9me2 between wild-type and *Cbx3*-KO spermatocytes. Relative fluorescence intensity of H3K9me2 against HP1β at PCH in *Cbx3*-KO was significantly reduced compared with wild type. The numbers of spermatocytes analyzed were as follows: wild type, *n*=92 from two mice; *Cbx3*-KO, *n*=60 from two mice at 15 dpp. The significance of the difference was evaluated using Student's *t*-test (P=1.37E^{-26}). Data are mean±s.e.m. (**C**) Normal level of H3K9me3 deposition at the PCH in *Cbx3*-KO spermatocytes at the leptotene stage. Immunofluorescence results for H3K9me3 (K9me3; green) and SYCP3 (white) with DAPI counterstaining (red) in wild-type and *Cbx3*-KO spermatocytes at the leptotene stage. The numbers of spermatocytes analyzed were as follows: wild type, *n*=100 from three mice; *Cbx3*-KO, *n*=150 from three mice at 15 dpp. Scale bars: 5 μm.

It is, however, known that Dnmt3b and Suv4-20h1/h2, an HMTase for H4K20, are potentially linked to H3K9me3 by HP1 proteins and thus could also contribute to progression of meiotic prophase (Lehnertz et al., 2003; Schotta et al., 2004). We, therefore, determined whether the *Cbx3* deficiency might influence DNA methylation status at the centromeric repeats and the silencing of their transcripts. We performed bisulfite DNA sequencing analysis and found that inactivation of *Cbx3* had no effect on overall DNA methylation in the minor satellite repeats and LINE1 (see Fig. S8A in the supplementary material; Y.T. and J.S., unpublished). Consistently, real-time PCR analysis for major and minor satellite and *LINE1* transcripts revealed no significant differences between *Cbx3*-heterozygote and *Cbx3*-KO germ cells (see Fig. S8B,C in the supplementary material). By notable contrast, we observed a complete loss of trimethylated H4K20 (H4K20me3) at PCH in all meiotic substages in the *Cbx3*-KO (see Fig. S9 in the supplementary material), suggesting that regulation of H4K20me3 during meiotic prophase is an additional role for HP1γ. It is, however, unlikely that H4K20me3 solely regulates the synapsis, which was shown to be impaired in *G9a*-KO cells despite normal H4K20me3 deposition at PCH (see Fig. S10 in the supplementary material). This implies that the HP1γ/G9a cascade is the dominant pathway by which H3K9me3 promotes proper synapsis.

HP1γ/G9a axis is involved in maintaining centromere clustering in early meiotic prophase

We went on to address how HP1γ regulates PCH functions. Centromeres are known to cluster in early meiotic prophase in a wide range of organisms, including mice (Stewart and Dawson, 2008). Although this process may play a role in the search for homologs that is required for subsequent chromosome synapsis, this role is poorly understood (Stewart and Dawson, 2008). In wild-type mice, centromere clustering was shown to occur as a punctate distribution at the nuclear periphery and has been observed as early as in intermediate and Type B spermatogonia, concurrent with loss of Plzf expression (Payne and Braun, 2006). It is noteworthy that this process was accompanied by induction of H3K9me2 and its punctate accumulation at the PCH. We thus hypothesized that the HP1γ/G9a cascade may mediate centromere clustering.

We first used whole-mount immunofluorescence of isolated seminiferous tubules to test whether the punctate deposition of H3K9me2 at the PCH depends on HP1γ. We found that in both *Cbx3*-hetero and *Cbx3*-KO, Plzf-/c-Kit+ differentiated spermatogonia extensively clustered, whereas Plzf+/c-Kit– undifferentiated spermatogonia formed small clusters composed of a few cells (Fig. 4A, indicated by yellow and white lines, respectively). Consistent with these results, an H3K9me2 signal was readily detectable at the DAPI-rich PCH in differentiated

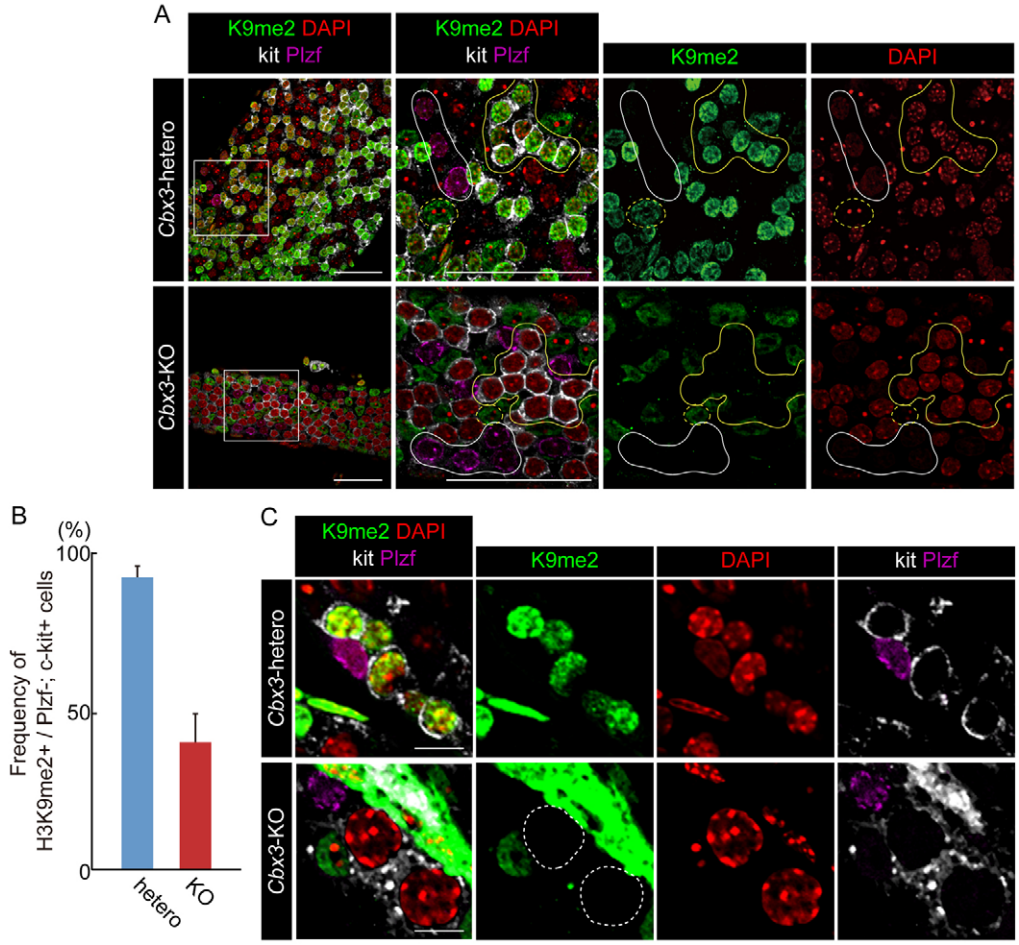

Fig. 4. Defects in H3K9me2 deposition in *Cbx3*-KO spermatogonia. (**A**) Defects in H3K9me2 deposition in c-kit positive spermatogonia in *Cbx3*-KO mice. Whole-mount immunostaining was performed on seminiferous tubules for H3K9me2 (K9me2; green), c-kit (white) and Plzf (magenta) with DAPI counterstaining (red) in 3-week-old *Cbx3*-hetero (upper panels) and *Cbx3*-KO mice (lower panels). Higher magnification views for the region indicated by boxes in the left panels are shown in the right panels. Clusters of Plzf+/c-kit– undifferentiated spermatogonia and Plzf-/c-kit+ differentiated spermatogonia are indicated by white and yellow lines, respectively. Broken yellow circles indicate Sertoli cells. Scale bars: 50 μm. (**B**) The number of H3K9me2-positive Plzf-/c-Kit+ differentiated spermatogonia was significantly reduced in *Cbx3*-KO compared with *Cbx3*-hetero. The numbers of spermatocytes analyzed were as follows: *Cbx3*-hetero, *n*=1092 from two mice; *Cbx3*-KO, *n*=595 from two mice at 21 dpp. The significance of the difference was evaluated using Student's *t*-test (P=1.34E^{-05}). Data are mean±s.e.m. (**C**) Punctate distribution of the PCH in the absence of H3K9me2 in differentiated spermatogonia of the *Cbx3*-KO. Immunofluorescence analysis was performed on testis sections for H3K9me2 (K9me2; green), c-kit (white) and Plzf (magenta) with DAPI counterstaining (red) in 3-week-old *Cbx3*-hetero (upper panels) and *Cbx3*-KO mice (lower panels). Plzf-/c-kit+ differentiated spermatogonia are indicated by broken lines in the lower panel. Scale bars: 10 μm.

spermatogonia but was hardly seen in the undifferentiated spermatogonia in adult *Cbx3*-hetero testis (Fig. 4A,B). We found that Plzf-/c-Kit+ spermatogonia were more frequent and densely populated in *Cbx3*-KO than in *Cbx3*-hetero mice due to the reduction of post-mitotic spermatocytes. The H3K9me2 signal in Plzf-/c-Kit+ differentiated spermatogonia in the *Cbx3*-KO was barely detectable, although the signal in Sertoli cells was similar to that in the *Cbx3*-hetero (Fig. 4A, broken yellow circles). We went on to test whether the punctate distribution of PCH was affected in *Cbx3*-KO and found no remarkable changes (Fig. 4C). Therefore, HP1γ is shown to mediate H3K9me2 at PCH as early as the differentiated spermatogonia stage, but is not required for punctate distribution of PCH at these stages.

We went on to investigate whether the *Cbx3* deficiency affects centromere clustering in early meiotic prophase, as an intense PCH distribution of H3K9me2 was continuously observed after entry into meiotic prophase. We performed immunofluorescence analysis for H3K9me3, anti-centromere antibody (ACA or CREST) and DAPI and counted the number of clusters. We chose areas in which H3K9me3, DAPI and CREST/ACA dots were all included as the centromeric clusters (indicated by broken lines in Fig. 5A). Labeling of leptotene cells with H3K9me3 and CREST or ACA revealed that centromere clustering was indeed disturbed; wild-type cells contained on average three to five clusters of heterochromatin, whereas in the *Cbx3*-KO the majority of cells contained six clusters or more (Fig. 5A,B). Consistent with the epistatic link of HP1γ with G9a, we found very similar defects in centromere clustering in *G9a*-KO spermatocytes (Fig. 5A,B). Based on these results, we suggest that the HP1γ/G9a axis is required to maintain the clustering of PCH and/or re-cluster the PCH at early in prophase, which may facilitate the synapsis.

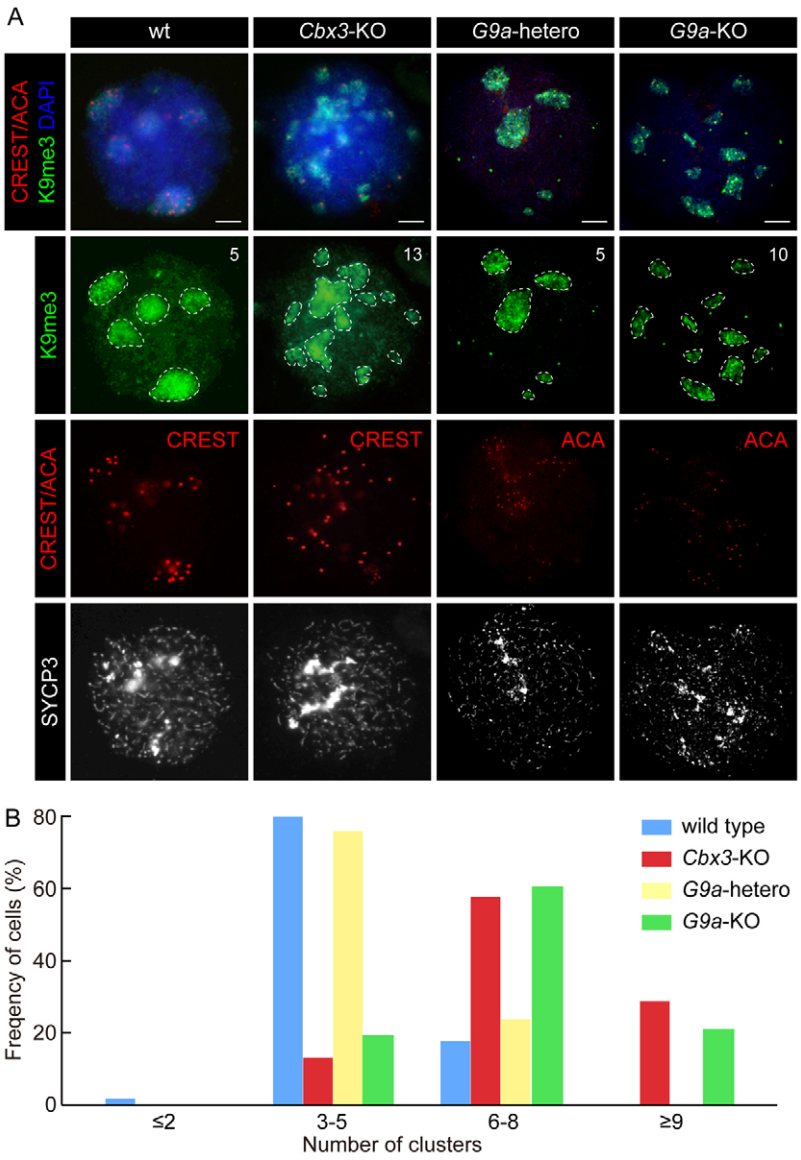

Fig. 5. Defects in centromere clustering at the leptotene stage in the *Cbx3*-KO and *G9a*-KO. (**A**) Defects in centromere clustering accompanied by scattered PCH in *Cbx3*-KO and *G9a*-KO at the leptotene stage. Immunofluorescence analysis was performed for anti-centromere antibody (CREST or ACA, red), H3K9me3 (K9me3; green) and SYCP3 (white) with DAPI counterstaining (blue) in spermatocytes from wild type and its littermate *Cbx3*-KO, and *G9a*-hetero and its littermate *G9a*-KO mice at the leptotene stage. Clusters in each nucleus are indicated by broken white lines. The number of clusters in each nucleus is indicated in the upper right-hand corner of each H3K9me3 (green) panel. The numbers of spermatocytes analyzed were as follows: wild type, *n*=49 from two mice; *Cbx3*-KO, *n*=79 from two mice; *G9a*-hetero, *n*=51 from two mice; and *G9a*-KO, *n*=81 from two mice at 15 dpp. Scale bars: 5 μm. (**B**) The degree of centromere clustering in wild-type, *Cbx3*-KO, *G9a*-hetero and *G9a*-KO leptotene spermatocytes. The number of centromere clusters was counted in each leptotene spermatocyte and the frequency of cells in each fraction is shown.

HP1γ facilitates homologous chromosome pairing

As homologous synapsis is initiated by chromosome pairing, we went on to examine whether HP1γ/G9a-dependent PCH clustering is involved in mediating the pairing. We used immunofluorescent in situ hybridization analysis to detect genomic regions close to the centromeric region of chromosome 2 (Chr2-Cen), together with SYCP3 and H3K9me3 to analyze the correlation between the pairing and PCH clustering (Fig. 6A). We also tested a non-centromeric genomic region in the middle part of chromosome 4 (Chr4-Mid) as a reference (see Fig. S11 in the supplementary material).

We first investigated wild-type pachytene spermatocytes, in which pairing is mostly completed, to determine the quantitative parameters that distinguish paired and unpaired homologous chromosomes (Fig. 6B; see Fig. S11 in the supplementary material). We found Chr2-Cen probes detected four or more speckles that associated with a single cluster of PCH. This may be due to the ~250 kb probe length, as 40 kb Chr4-Mid probes always detected four speckles. In both cases, four or more speckles were located in close proximity. Average distances between the most separated speckles were 4.6±1.8 μm for Chr2-Cen probe and 3.3±1.3 μm for Chr4-Mid probe at this stage. By contrast, at the leptotene and zygotene stages, we frequently found two clusters of paired speckles, which may represent cohesion of sister chromatids, at each genomic region. These two clusters were separated more than 10 μm on average at the leptotene stage and became slightly closer at zygotene. Based on these observations, we arbitrarily identified paired chromosomal regions as clusters of four or more speckles in which all speckles were located within a distance of no more than 6.4 or 4.6 μm (mean+1 s.d.) for Chr2-Cen and Chr4-mid, respectively (Fig. 6B; see Fig. S11 in the supplementary material).

We then investigated how homologous chromosome pairing progressed in meiotic spermatocytes by using these criteria. The Chr2-Cen region was shown to pair in 23% and 44% of meiotic spermatocytes paired at the leptotene and zygotene stages, respectively, and almost 100% at the pachytene (Fig. 6C). We also observed that the pairing at Chr4-Mid region progressed in a similar fashion (see Fig. S11 in the supplementary material). These results are reminiscent of previous observations on proximal X chromosomes in early female mouse meiosis (O'Keeffe et al., 1997). We went on to examine the pairing progression in *Cbx3*-KO

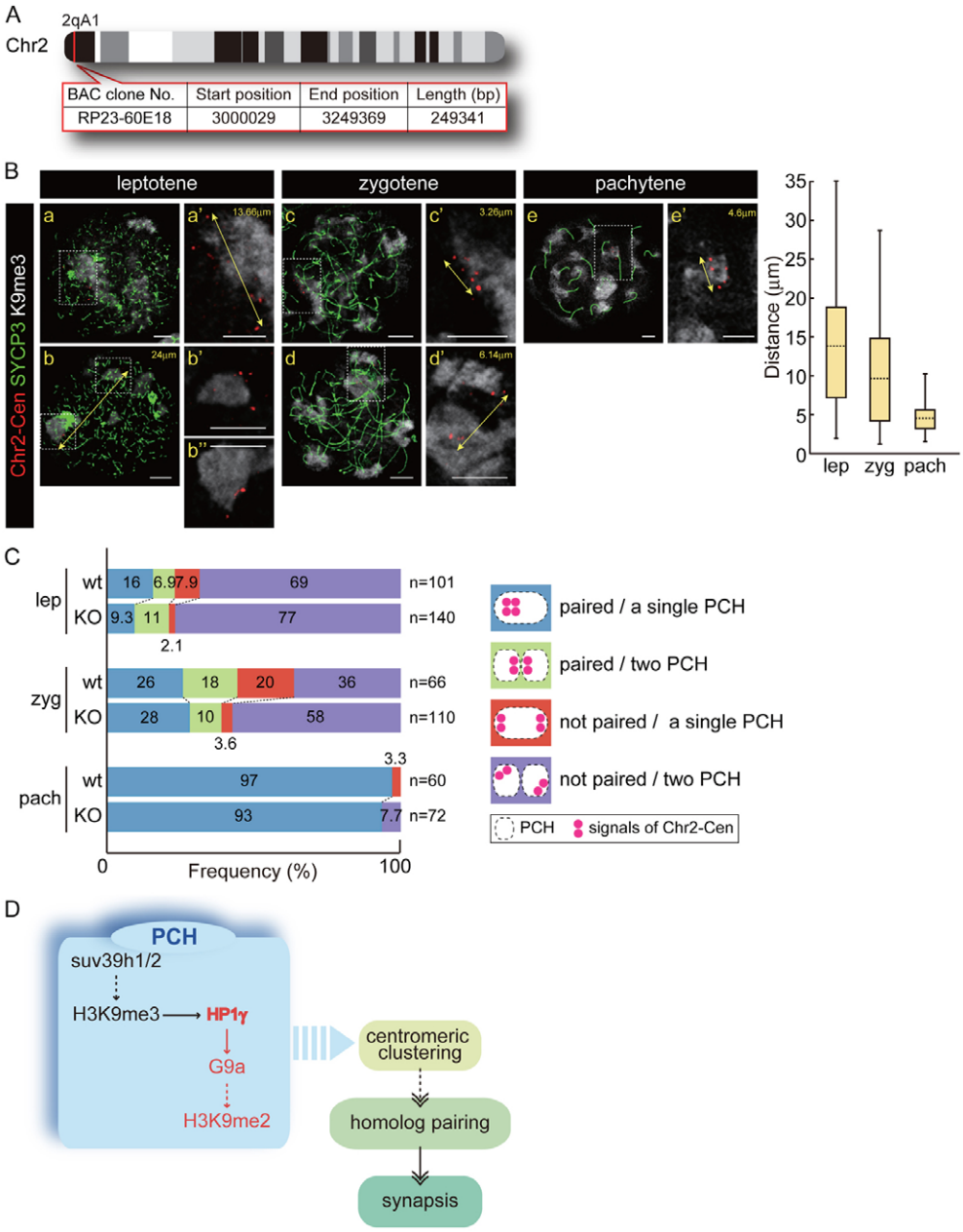

Fig. 6. PCH-mediated early meiotic prophase centromere clustering of unpaired homologous chromosomes is impaired in the *Cbx3*-KO. (**A**) Genomic position and properties of the probe to detect a genomic region close to centromeric region of chromosome 2 (Chr2-Cen). BAC clone, RP23-60E18, was used to generate the fluorescent in situ hybridization probe. This probe detects 2qA1 region on chromosome 2 (shown by the red bar). (**B**) Progression of pairing at the Chr2-Cen region. Representative results of immunofluorescent in situ hybridization analysis for Chr2-Cen probe (red), SYCP3 (green) and H3K9me3 (K9me3; white) on meiotic cell spreads from wild type at the leptotene (a,b), zygotene (c,d) and pachytene (e) stages are shown (left panels). Higher magnification views for the PCH indicated by broken white boxes in a to e are shown in a′ to e′, respectively, with fluorescent in situ hybridization signals. The most separated Chr2-Cen signals in each spermatocyte are indicated by yellow double-headed arrows in each panel and their distances are also shown. Average distances of the most separated Chr2-Cen signals at each stage were determined and are graphically depicted (right panel). The broken line in each box represents the average distance (leptotene, 13.9 μm; zygotene, 9.7 μm; pachytene, 4.6 μm) and s.d., respectively. The numbers of spermatocytes analyzed were as follows: leptotene, *n*=110; zygotene, *n*=66; pachytene, *n*=56 (from two wild-type mice at 15 dpp). Scale bars: 5 μm. Error bars indicate the range of measurement data. (**C**) Defects in association of unpaired Chr2-Cen regions with a single PCH in *Cbx3*-KO. We examined pairing of Chr2-Cen regions and their association with a single or two PCH in each spermatocyte of wild type (wt) and *Cbx3*-KO (KO). We identified pairing of the Chr2-Cen region when four or more signals are not separated more than 6.4 μm (mean + 1 s.d.). Based on these parameters, spermatocytes are classified into four categories, as shown in the right-hand panel. We determined the frequency of cells included in each category at each stage and show the results graphically (left). The following color codes are used: blue, Chr2-Cen regions were paired and associated with a single PCH; green, Chr2-Cen regions were paired and associated with two PCH; red, Chr2-Cen regions were not paired and associated with a single PCH; purple, Chr2-Cen regions were not paired associated with two PCH. The numbers (n) of spermatocytes analyzed at each stage are indicated. (**D**) Schematic summary for this study. Sequential epigenetic modifications at PCH that occur in early meiotic prophase are shown on the left. HP1γ is identified as a link between H3K9me3 and H3K9me2. The HP1γ/G9a cascade at PCH is required to maintain centromere clustering early in prophase, which may facilitate homologous chromosome pairing and synapsis.

and, to our surprise, did not find obvious difference at either genomic region in comparison with the wild type. This indicates that HP1γ is dispensable for the homology search at both centromeric and middle regions of the chromosome and is indeed consistent with a previous report showing initiation of synapsis at multiple points along the mouse chromosome (Liebe et al., 2004). Although the pairing in *Cbx3*-KO spermatocytes seemingly progressed in a manner similar to the wild type, this is likely to represent the consequence of considerable depletion of mutant spermatocytes during early meiotic prophase. We therefore assume that meiotic spermatocytes that failed to undergo a certain extent of pairing at each stage might be preferentially deleted during early prophase, presumably by quality control mechanisms. Consistent with this model, synaptic defects in *Cbx3*-KO spermatocytes that survived up to the pachytene stage were only seen in limited chromosomal regions (Table 1). We thus suggest a role for HP1γ to facilitate the pairing.

We then examined whether HP1γ-dependent PCH clustering was involved to facilitate the homology search. To this end, we tested the correlation between PCH-clustering and the pairing by scoring the number of cells, in which Chr2-Cen regions were paired and/or associated with a single PCH, at each stage (Fig. 6C). Analyses of wild-type spermatocytes revealed that pairing of the Chr2-Cen region was not always accompanied by association with a single PCH or vice versa at leptotene or zygotene stages, whereas they mostly coincided at pachytene (see panels a to d in Fig. 6B and summary in 6C). This may reflect the plastic and dynamic nature of PCH clustering during the homology search. Consistent with defects in PCH clustering in *Cbx3*-KO mice, association of four or more Chr2-Cen speckles with a single PCH was seen in only 11% of leptotene spermatocytes compared with 24% in the wild type. We further observed considerable differences between the wild type and *Cbx3*-KO at leptotene and zygotene stages in the frequency of spermatocytes in which the Chr2-Cen regions were associated with a single PCH but did not pair (a category represented by panel a in Fig. 6B). This fraction represented 8% at leptotene and 20% at zygotene in the wild type, but was reduced to 2.1% and 3.6%, respectively, in the *Cbx3*-KO. This suggests that HP1γ contributes to retain centromeric regions of unpaired homologous chromosomes in a single PCH, probably by maintaining their clustering and keeping them in close alignment before they pair.

DISCUSSION

Our data support the model that Suv39h1/h2-catalyzes the trimethylation of histone H3K9 at PCH, which then acts as a platform for HP1γ localization. HP1γ in turn recruits G9a, which mediates transient acquisition of the H3K9me2 mark at PCH in differentiated spermatogonia and spermatocytes. HP1γ is thus identified as a functional link for sequential H3K9 epigenetic modifications at PCH that are required for proper progression of meiosis (Fig. 6D). Consistently, centromere clustering at early meiotic prophase and subsequent homologous synapsis are commonly affected in *Cbx3* and *G9a* mutant spermatocytes. Finally, we show that HP1γ/G9a-dependent PCH clustering is not essential for the pairing but crucially facilitates homologous chromosome interactions by keeping their centromeric regions in close proximity irrespective of their pairing status in early meiotic prophase. The HP1γ/G9a cascade is also dispensable for centromere clustering in differentiated spermatogonia (Fig. 4). This differential requirement implies that potential mechanisms that unsettle the centromere clustering begin operating once germ cells enter meiosis and are balanced by HP1γ/G9a-dependent mechanisms to cluster centromeres at PCH. Intriguingly, such bipartite functions of meiotic centromeres have been previously shown in budding yeast. Here, centromeres serve as sites of homology-independent initial chromosomal association and as sites for the later synapsis initiation that occurs upon their homologous coupling. They are also the site of a destructive disjunction that occurs upon failure of chromosomal cross over (Tsubouchi and Roeder, 2005; Tsubouchi et al., 2008). The HP1γ/G9a cascade is therefore likely to be involved in mediating evolutionarily conserved functions of meiotic centromeres for correct homologous partner choice to initiate synapsis.

Based on genome-wide analysis of its distribution, dimethylated H3K9 has recently been suggested to play a role in regulation of chromosome dynamics because of the existence of large blocks of heterochromatin in differentiated cells that are dimethylated at H3K9 (Wen et al., 2009). These regions overlap significantly with previously described large nuclear lamina-associated domains (Guelen et al., 2008). Based on these observations, Wen and colleagues proposed that H3K9me2 marks would bring these large genomic regions close to the nuclear lamina (Wen et al., 2009). Similarly, HP1γ-dependent H3K9me2 at the PCH probably links meiotic centromeres to each other to facilitate synapsis. Our study thus provides the first functional evidence for the role of PCH with H3K9me2 marks for stage-specific regulation of chromosome dynamics, although the mechanisms for recognition of H3K9me2 still await discovery.

This study also provides insight into functional correlations of two different H3K9 methylation marks. Previous studies, in which ES cells and embryonic fibroblasts were used, demonstrated that H3K9me2 and H3K9me3 are localized to distinct silent domains: H3K9me2 was enriched within silent euchromatic regions whereas H3K9me3 was enriched at PCH (Lehnertz et al., 2003; Tachibana et al., 2002; Tachibana et al., 2005). Our study clearly indicates that this distinction is conditional. In particular, acquisition of H3K9me2 marks seems to be flexible, in contrast to the constitutive deposition of H3K9me3 at PCH, and thus may not solely rely on genomic signatures. Concordant with this interpretation, G9a is reported to form complexes with not only HP1γ but also with other proteins such as Wiz and Np95 (Estève et al., 2006; Ueda et al., 2006). These interactions may aid in the recognition of various epigenetic configurations by G9a and enable local and conditional deposition of H3K9me2. Our study thus reveals considerable plasticity in the interplay between different histone modifications, and suggests that such stepwise and dynamic epigenetic modifications may play a pivotal role during differentiation and/or cell cycle progression.

Funding

This work was supported by Grants-in-aid from the Ministry of Education, Culture, Sports, Science and Technology (MEXT) of Japan to H.K. and M.A. Y.T. and J.S. are supported by Special Postdoctoral Researcher Program of RIKEN.

Competing interests statement

The authors declare no competing financial interests.

Supplementary material

Supplementary material for this article is available at http://dev.biologists.org/lookup/suppl/doi:10.1242/dev.064444/-/DC1

References

Bannister, A. J., Zegerman, P., Partridge, J. F., Miska, E. A., Thomas, J. O., Allshire, R. C. and Kouzarides, T. (2001). Selective recognition of methylated lysine 9 on histone H3 by the HP1 chromo domain. *Nature* **410**, 120-124.

Brown, J. P., Bullwinkel, J., Baron-Lühr, B., Billur, M., Schneider, P., Winking, H. and Singh, P. B. (2010). HP1gamma function is required for male germ cell survival and spermatogenesis. *Epigenetics Chromatin* **3**, 9.
Cheutin, T., McNairn, A. J., Jenuwein, T., Gilbert, D. M., Dingh, P. B. and Misteli, T. (2003). Maintenance of stable heterochromatin domains by dynamic HP1 binding. *Science* **299**, 721-725.
Dernburg, A. F., Sedat, J. W. and Hawley, R. S. (1996). Direct evidence of a role for heterochromatin in meiotic chromosome segregation. *Cell* **86**, 135-146.
Ding, D. Q., Yamamoto, A., Haraguchi, T. and Hiraoka, Y. (2004). Dynamics of homologous chromosome pairing during meiotic prophase in fission yeast. *Dev. Cell* **6**, 329-341.
Ekwall, K., Nimmo, E. R., Javerzat, J. P., Borgstrom, B., Egel, R., Cranston, G. and Allshire, R. (1996). Mutations in the fission yeast silencing factors Clr4+ and rik1+ disrupt the localization of the chromo domain protein Swi6p and impair centromere function. *J. Cell Sci.* **109**, 2637-2648.
Estève, P. O., Chin, H. G., Smallwood, A., Feehery, G. R., Gangisetty, O., Karpf, A. R., Carey, M. F. and Pradhan, S. (2006). Direct interaction between DNMT1 and G9a coordinates DNA and histone methylation during replication. *Genes Dev.* **20**, 3089-3103.
Guelen, L., Pagie, L., Brasset, E., Meuleman, W., Faza, M. B., Talhout, W., Eussen, B. H., de Klein, A., Wessels, L., de Laat, W. et al. (2008). Domain organization of human chromosomes revealed by mapping of nuclear lamina interaction. *Nature* **453**, 948-951.
Jenuwein, T. and Allis, C. D. (2001). Translating the histone code. *Science* **293**, 1074-1080.
Kellum, R. and Alberts, B. M. (1995). Heterochromatin protein 1 is required for correct chromosome segregation in *Drosophila* embryos. *J. Cell Sci.* **108**, 1419-1431.
Kemp, B., Boumil, R. M., Stewart, M. N. and Dawson, D. S. (2004). A role for centromere pairing in meiotic chromosome segregation. *Genes Dev.* **18**, 1946-1951.
Khalil, A. M., Boyar, F. Z. and Driscoll, D. J. (2004). Dynamic histone modifications mark sex chromosome inactivation and reactivation during mammalian spermatogenesis. *Proc. Natl. Acad. Sci. USA* **101**, 16583-16587.
Lachner, M., O'Carroll, D., Rea, S., Mechtler, K. and Jenuwein, T. (2001). Methylation of histone H3 lysine 9 creates a binding site for HP1 proteins. *Nature* **410**, 116-120.
Lammers, J. H., Offenberg, H. H., van Aalderen, M., Vink, A. C., Dietrich, A. J. and Heyting, C. (1994). The gene encoding a major component of the lateral elements of synaptonemal complexes of the rat is related to X-linked lymphocyte-reduced genes. *Mol. Cell. Biol.* **14**, 1137-1146.
Lehnertz, B., Ueda, Y., Derijck, A. A., Braunschweig, U., Perez-Burgos, L., Kubicek, S., Chen, T., Li, E., Jenuwein, T. and Peters, A. H. (2003). Suv39h-mediated histone H3 lysine 9 methylation directs DNA methylation to major satellite repeats at pericentric heterochromatin. *Curr. Biol.* **13**, 1192-1200.
Liebe, B., Alsheimer, M., Höög, C., Benavente, R. and Scherthan, H. (2004). Telomere attachment, meiotic chromosome condensation, pairing, and bouquet stage duration are modified in spermatocytes lacking axial elements. *Mol. Biol. Cell* **15**, 827-837.
Lomberk, G., Wallrath, L. and Urrutia, R. (2006). The heterochromatin protein 1 family. *Genome Biol.* **7**, 228.1-228.7.
Metzler-Guillemain, C., Luciani, J., Depetris, D., Guichaoua, M. R. and Mattei, M. G. (2003). HP1beta and HP1gamma, but not HP1alpha, decorate the entire XY body during human male meiosis. *Chromosome Res.* **11**, 73-81.
Meuwissen, R. L., Offenberg, H. H., Dietrich, A. J., Riesewijk, A., van Iersel, M. and Heyting, C. (1992). A coiled-coil related protein specific for synapsis regions of meiotic prophase chromosomes. *EMBO J.* **11**, 5091-5100.
Nakashima, H., Nakano, M., Ohnishi, R., Hiraoka, Y., Kaneda, Y., Sugino, A. and Masumoto, H. (2005). Assembly of additional heterochromatin distinct from centromere-kinetochore chromatin is required for de novo formation of human artificial chromosome. *J. Cell Sci.* **118**, 5885-5898.
Nakayama, J., Ricem, J. C., Strahl, B. D., Allis, C. D. and Grewal, S. I. (2001). Role of histone H3 lysine 9 methylation in epigenetic control of heterochromatin assembly. *Science* **292**, 110-113.
Naruse, C., Fukusumi, Y., Kakiuchi, D. and Asano, M. (2007). A novel gene trapping for identifying genes expressed under the control of specific transcription factors. *Biochem. Biophys. Res. Commun.* **361**, 109-115.
O'Keeffe, C., Hultèn, M. A. and Tease, C. (1997). Analysis of proximal X chromosome pairing in early female mouse meiosis. *Chromosoma* **106**, 276-283.
Ogawa, H., Ishiguro, K., Gaubatz, S., Livingston, D. M. and Nakatani, Y. (2002). A complex with chromatin modifiers that occupies E2F- and Myc-responsive genes in G_0 cells. *Science* **296**, 1132-1136.
Ohmura, M., Yoshida, S., Ide, Y., Nagamatsu, G., Suda, T. and Ohbo, K. (2004). Spatial analysis of germ stem cell development in Oct-4/EGFP transgenic mice. *Arch. Histol. Cytol.* **67**, 285-296.
Payne, C. and Braun, R. E. (2006). Histone lysine trimethylation exhibits a distinct perinuclear distribution in Plzf-expressing spermatogonia. *Dev. Biol.* **293**, 461-472.
Peters, A. H., Plug, A. W., van Vugt, M. J. and de Boer, P. (1997). A drying-down technique for the spreading of mammalian meiocytes from the male and female germline. *Chromosome Res.* **5**, 66-68.
Peters, A. H., O'Carroll, D., Scherthan, H., Mechtler, K., Sauer, S., Schöfer, C., Weipoltshammer, K., Pagani, M., Lachner, M., Kohlmaier, A. et al. (2001). Loss of the Suv39h histone methyltransferases impairs mammalian heterochromatin and genome stability. *Cell* **107**, 323-337.
Pidoux, A. L. and Allshire, R. C. (2005). The role of heterochromatin in centromere function. *Philos. Trans. R. Soc. B* **360**, 569-579.
Prieto, P., Santos, A. P., Moore, G. and Shaw, P. (2004). Chromosomes associate premeiotically and in xylem vessel cells via their telomeres and centromeres in diploid rice (*Oryza sativa*). *Chromosoma* **112**, 300-307.
Sato, M., Miyado, K. and Kimura, M. (2001). Cloning and characterization of 5′-upstream sequence of the M32 gene for a mouse homologue of *Drosophila* heterochromatin protein 1 (HP1). *DNA Seq.* **12**, 97-106.
Schotta, G., Lachner, M., Sarma, K., Ebert, A., Sengupta, R., Reuter, G., Reinberg, D. and Jenuwein, T. (2004). A silencing pathway to induce H3-K9 and H4-K20 trimethylation at constitutive heterochromatin. *Genes. Dev.* **18**, 1251-1262.
Sharif, J., Muto, M., Takebayashi, S., Suetake, I., Iwamatsu, A., Endo, T. A., Shinga, J., Mizutani-Koseki, Y., Toyoda, T., Okamura, K. et al. (2007). The SRA protein Np95 mediates epigenetic inheritance by recruiting Dnmt1 to methylated DNA. *Nature* **450**, 908-912.
Stewart, M. N. and Dawson, D. S. (2008). Changing partners: moving from non-homologous to homologous centromere pairing in meiosis. *Trends Genet.* **24**, 564-573.
Tachibana, M., Sugimoto, K., Nozaki, M., Ueda, J., Ohta, T., Ohki, M., Fukuda, M., Takeda, N., Niida, H., Kato, H. et al. (2002). G9a histone methyltransferase plays a dominant role in euchromatic histone H3 lysine 9 methylation and is essential for early embryogenesis. *Genes Dev.* **16**, 1779-1791.
Tachibana, M., Ueda, J., Fukuda, M., Takeda, N., Ohta, T., Iwanari, H., Sakihama, T., Kodama, T., Hamakubo, T. and Shinkai, Y. (2005). Histone methyltransferases G9a and GLP form heterochromatic complexes and are both crucial for methylation of euchromatin at H3-K9. *Genes Dev.* **19**, 815-826.
Tachibana, T., Nozaki, M., Takeda, N. and Shinkai, Y. (2007). Functional dynamics of H3K9 methylation during meiotic prophase progression. *EMBO J.* **26**, 3346-3359.
Tsubouchi, T. and Roeder, S. (2005). A synaptonemal complex protein promotes homology-independent centromere coupling. *Science* **308**, 870-873.
Tsubouchi, T., Macqueen, A. J. and Roeder, S. (2008). Initiation of meiotic chromosome synapsis at centromeres in budding yeast. *Genes Dev.* **22**, 3217-3226.
Ueda, J., Tachibana, M., Ikura, T. and Shinkai, Y. (2006). Zinc finger protein Wiz links G9a/GLP histone methyltransferases to the co-repressor molecule CtBP. *J. Biol. Chem.* **281**, 20120-20128.
Wen, B., Wu, H., Shinkai, Y., Irizarry, R. A. and Feinberg, A. P. (2009). Large histone H3 lysine 9 dimethylated chromatin blocks distinguish differentiated from embryonic stem cells. *Nat. Genet.* **41**, 246-250.
Williams, S., Mustoe, T., Mulcahy, T., Griffiths, M., Simpson, D., Antoniou, M., Irvine, A., Mountain, A. and Crombie, R. (2005). CpG-island fragments from the HNRPA2B1/CBX3 genomic locus reduce silencing and enhance transgene expression from the hCMV promoter/enhancer in mammalian cells. *BMC Biotechnol.* **3**, 5-17.